NJC

RSC Publishing

PAPER

View Article Online
View Journal | View Issue

Cite this: *New J. Chem.*, 2013, **37**, 1728

A facile strategy to enhance the fill factor of ternary blend solar cells by increasing charge carrier mobility

Kun Lu,[a] Jin Fang,[a] Xiangwei Zhu,[a] Han Yan,[a] Denghua Li,[a] Chong'an Di,[b] Yanlian Yang[a] and Zhixiang Wei*[a]

Received (in Montpellier, France) 16th November 2012, Accepted 2nd January 2013

DOI: 10.1039/c2nj41039g

www.rsc.org/njc

Two conjugated polymers based on benzo[1,2-*b*:4,5-*b*′]dithiophene (BDT) with triethylene glycol (TEG) and ethylhexyl side chains (abbreviated as PBDTT-TEG and PBDTT-EH, respectively) were designed and synthesized. A polymer field-effect transistor of PBDTT-TEG exhibited a charge carrier mobility nearly one order of magnitude higher than that of PBDTT-EH. Measurements on polymer solar cells (PSCs) based on polymer:[6,6]-phenyl-C_{71}-butyric acid methyl ester ($PC_{71}BM$) binary blends showed the PBDTT-TEG-based devices had higher short-circuit current density (J_{sc}) than PBDTT-EH. The effect of the incorporation of PBDTT-TEG into PBDTT-EH on the photovoltaic properties has been investigated by blending them together with different ratios. The optimization of the devices showed an obvious increase in fill factor (FF) values and an improvement in efficiency compared with their binary ones, which is ascribed to a higher charge mobility and higher crystallinity of PBDTT-TEG.

1. Introduction

Over the past decades, significant progress has been made on π-conjugated polymers due to their excellent optoelectronic properties and potential applications in bulk heterojunction (BHJ) polymer solar cells (PSCs), polymer field-effect transistors (PFETs) and light-emitting diodes.[1–4] Specifically, PSCs have drawn worldwide attention during the last ten years for their potential as a green, flexible, and low-cost renewable energy source.[2,3,5–8] With more recently developed polymer materials, high power conversion efficiencies (PCEs) of 6–9% have been demonstrated.[9–11]

As an efficient route toward application of PSCs, blending is a commonly employed strategy in the manufacturing of commodity polymer products to enhance their performance, reduce cost, and impart additional functionalities.[12–14] At present, most PSCs are based on polymer–fullerene binary blends and most efforts are made to search for alternative donor polymers. However, the parameters of binary blend BHJ PSCs are usually difficult to tune, limited by single donor polymer. Blending multiple donor components with different properties into one PSC is an alternative method. Recently, this simple method has been successfully demonstrated by the addition of a small fraction of dye molecules or a small band gap polymer into the archetypical poly(3-hexylthiophene)/[6,6]-phenyl-C-butyric acid methyl ester (PCBM) BHJ cells.[15,16] Although ternary blend solar cells have received far less attention, they have been recognized as a potential route to increase the efficiency while retaining the simplicity of a single active-layer processing step.[12,13,17–19] Despite this potential advantage, it has been proposed that one of the drawbacks of them was that the fill factor (FF) would not be high enough for the compatibility of the polymers, thus limiting the perceived impact of this device platform.[13,20] Generally, polymer–polymer blends have a strong, entropy-driven, tendency towards phase separation.[14] To date, using two p-type conjugated polymers in one PSC has not been extensively explored due to their immiscibility and phase separation problems, although a few examples could achieve high FF values in this polymer–polymer–fullerene ternary system.[21,22] Mixing of two polymers might disturb the chain stacking in the solid state. The other aspect is the mismatch of energy levels for the two polymers which may inhibit charge transfer in their blending state.

One of the efficient routes to improve FF values of PSCs is enhancing the carrier mobility of the donor polymers.[23] As a typical π-conjugation unit, benzo[1,2-*b*:4,5-*b*′]dithiophene (BDT) has been demonstrated to be one of the most excellent building blocks for the synthesis of organic functional materials.[24,25] BDT has a symmetric and planar conjugated structure, and hence tight stacking can be expected for the BDT-based conjugated polymers. Therefore, BDT-based polymers usually gain a high

[a] *National Center for Nanoscience and Technology, Beijing, 100190, China. E-mail: weizx@nanoctr.cn; Fax: +86 10 62656765; Tel: +86 10 82545565*

[b] *Institute of Chemistry, Chinese Academy of Sciences, Beijing, 100190, China. Fax: +86 10 625536989; Tel: +86 10 62552061*

carrier mobility.[11,24,26] In the research of conjugated polymers, side chains modifying the backbones is one of the important aspects for optoelectronic applications.[27–30] Previous works found that alkoxy side chains, especially triethylene glycol (TEG) chains, had several advantages over alkyl analogous.[31–33] The first is that if the oxygen is directly attached to the fused ring, the bandgap of the polymer can be reduced by a substantial amount. The second is that alkoxy side chains will not cause a detrimental steric twist of the polymer out of planarity which is beneficial for charge transport and can lead to high carrier mobility. The third is alkoxy side chains generally lead to good crystallinity which is important to film morphology.[31–34] TEG has been densely used in optoelectronic applications, and are proved to be a benefit to promote device performance.[34–40] In photovoltaic applications, TEG derivatives are usually used to modify electrodes as a buffer layer for improving the contact of organic/metal interfaces and enhance the open circuit voltage (V_{oc}) values.[36,39,40] There are also some works reporting that TEG-modified fullerenes, which could self-segregate to the surface of the blend film forming an ideal vertical morphology, could improve the efficiency and stability of the PSCs.[35]

In this paper, two polymers with TEG and ethylhexyl-substituted BDT coupling with thiophene units (PBDTT-TEG and PBDTT-EH, respectively) were designed and synthesized through a Stille coupling reaction. The synthetic route is shown in Scheme 1. The similarity in the chemical structures of the polymers was envisioned to give good miscibility between them. The ethylhexyl side chains on the BDT unit enhanced the solubility, while the linear TEG side chains led to a lower solubility in orthodichlorobenzene (ODCB). Both the two polymers were soluble in chloroform. The PFETs and PSCs were then fabricated and characterized. Consequently, ternary PSCs were fabricated to improve the photovoltaic performance by altering the blending ratios of two polymers. The absorption spectra, energy levels, and film morphology were then investigated in order to emphasize the effects of the structural factors on the charge transfer and photovoltaic properties of polymers.

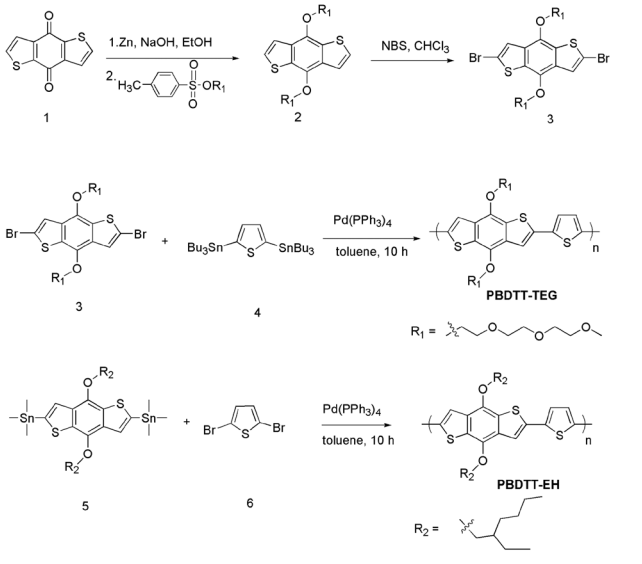

Scheme 1 Synthetic route of the polymers.

2. Experimental section

2.1 Instruments

^{1}H-NMR (400 MHz) spectra were obtained on a Bruker DMX-400 NMR Spectrometer using tetramethylsilane as internal standard. MS spectra (MALDI-TOF-MS) were determined on Micromass GCT-MS spectrometer. The electrochemical cyclic voltammetry was conducted on an electrochemical workstation (VMP3 Biologic, France) with Pt disk coated with the polymer film, Pt plate, and Ag/Ag^+ electrode as working electrode, counter electrode and reference electrode respectively in a 0.1 mol L^{-1} tetrabutylammonium hexafluorophosphate (Bu_4NPF_6) acetonitrile solution. AFM images of the blend films prepared by spin coating 10 mg mL^{-1} polymer:[6,6]-phenyl-C_{71}-butyric acid methyl ester ($PC_{71}BM$) solutions in dry dichlorobenzene on the indium/tin oxide (ITO) substrates were obtained on a Nanoscope IIIa AFM (Digital Instruments) in tapping mode. XRD measurements were carried out in the reflection mode at room temperature using a 12-Kw D/max-rA X-ray diffraction system. The step size for all scans was 1 degree with a count time of 1 min per step. The thickness of the active layer was controlled by changing the spin speed during the spin-coating process and measured on a Kla-Tencor D–120 profilometer. The *J–V* curves were obtained by a Keithley 2420 source-measure unit. The photocurrent was measured under illumination using an Oriel Newport 150W solar simulator (AM 1.5G), and the light intensity was calibrated with a Newport reference detector (Oriel PN 91150V). The EQE measurements of the devices were performed in air with an Oriel Newport system (Model 66902).

2.2 Synthesis

Materials. All reagents and chemicals were purchased from Aldrich, Alfa and used as received. Solvents and other common reagents were obtained from the Beijing Chemical Plant. Toluene, chloroform and tetrahydrofuran (THF) were freshly distilled prior to use. The other materials were used without further purification. TEG monomethyl ether, 2,5-bis(tributylstannyl)thiophene (**4**), 2,5-dibromothiophene (**6**) were purchased from Aldrich and used as received. benzo[1,2-*b*:4,5-*b*′]dithiophen-4,8-dione (**1**) was prepared according to the literature procedures.[41]

4,8-Bis(2-TEG)benzo[1,2-*b*:4,5-*b*′]dithiophene (2). Compound **2** was prepared according to the literature procedures.[11] The benzo[1,2-*b*:4,5-*b*′]dithiophen-4,8-dione (1.0 g, 4.5 mmol) was mixed with zinc dust (0.65 g, 10 mmol) in a flask. Ethanol (4 mL) and NaOH solution (15 mL, 20%) were added, and the mixture was refluxed for 1 h. 2-TEG *p*-toluenesulfonate was added in portions with stirring until the color changed to red. The resulting precipitate was filtered and the filtrate was diluted with 100 mL of water and extracted with chloroform (100 mL). The organic extraction was dried with anhydrous sodium sulfate and evaporated in vacuum. Column chromatography on silica gel using dichloromethane and hexanes mixed eluents yielded the compound as light yellow oil. Yield = 45%.

MS (MALDI): *m*/*z*. 514 ^{1}H NMR ($CDCl_3$, 400 MHz): δ (ppm) = 7.67–7.65 (d, 2H), 7.36–7.35 (d, 2H), 4.44–4.43 (t, 4H), 3.88–3.86 (t, 4H), 3.78–3.75 (t, 4H), 3.73–3.71 (t, 4H), 3.70–3.68 (t, 4H), 3.66–3.55 (t, 4H), 3.38 (s, 6H).

4,8-Bis(2-ethylhexyloxy)benzo[1,2-*b*:4,5-*b*′]dithiophene. This compound was synthesized according to the procedures above. Yield = 40%. MS: *m*/*z*. 447 ^{1}H NMR ($CDCl_3$, 400 MHz): δ (ppm) = 7.50–7.46 (d, 2H), 7.36–7.32 (d, 2H), 3.97–3.84 (m, 4H), 1.62–1.50 (m, 2H), 1.38–1.10 (m, 16H), 0.90–0.72 (m, 12H).

2,6-Dibromo-4,8-Bis(2-TEG)benzo[1,2-*b*:4,5-*b*′] dithiophene (3). 2.57 g (5.0 mmol) 4,8-Bis(2-TEG)benzo[1,2-*b*:4,5-*b*′] dithiophene in $CHCl_3$ (20 mL) was reacted with 2 g (11.2 mmol) NBS and 2 mL acetic acid at room temperature overnight. The light gray suspension was treated with water and filtered off. After silica column chromatography with hexane, 2.95 g pale white solid was obtained, yield = 88%. MS (MALDI): *m*/*z*. 670 ^{1}H NMR ($CDCl_3$, 400 MHz): δ (ppm) = 7.55 (s, 2H), 4.35–4.33 (t, 4H), 3.85–3.82 (t, 4H), 3.76–3.73 (t, 4H), 3.72–3.69 (t, 4H), 3.58–3.56 (t, 4H), 3.38 (s, 6H).

2,6-Bis(trimethyltin)-4,8-bis(2-ethylhexyloxy)benzo[1,2-*b*:4,5-*b*′]dithiophene (5). This compound was prepared according to the literature procedures.[23] 4,8-Bis(2-ethylhexyloxy)benzo-[1,2-*b*:4,5-*b*′]dithiophene (0.62 g, 1.4 mmol) was dissolved in 20 mL of anhydrous THF and cooled in an acetone/dry ice bath under nitrogen protection. Butyllithium solution (1.4 mL, 3.5 mmol) was added dropwise with stirring, after the addition the mixture was kept in a dry ice bath for 30 min and at room temperature for 30 min. The mixture was cooled in the dry ice bath and trimethyltin chloride solution (4.2 mL, 4.2 mmol, 1 M in THF) was added, and the mixture was stirred at room temperature overnight. The mixture was quenched with 50 mL of water and extracted with hexanes. The organic extraction was dried with anhydrous sodium sulfate and evaporated *in vacuo.* Recrystallization of the residue from ethanol yielded the compound **5** as colorless needles, yield = 80%. MS (MALDI): *m*/*z*. 774 ^{1}H NMR ($CDCl_3$, 400 MHz): δ (ppm) = 7.51 (t, 2H), 4.23–4.15 (d, 4H), 1.58–1.54 (m, 4H), 1.35–1.33 (m, 18H), 1.10–0.90 (m, 12H), 0.43 (s, 18H).

General method of polymerization. The polymerization was prepared according to the literature procedures.[42] $Pd(PPh_3)_4$ (50 mg, 0.043 mmol), compound **3** and **4** (1 mmol), or compound **5** and **6** (1 mmol) were put into a three-neck flask. The mixture was flushed with argon for 10 min and then 10 mL toluene was added. Under the protection of argon, the reactant was heated to reflux for 18 h. The mixture was cooled to room temperature and a solution of KF (5 g) in water (10 mL) was added and stirred at room temperature for 2 h to remove the tin impurity. The mixture was extracted with toluene (2 × 150 mL), washed with water (2 × 150 mL), and dried over anhydrous $MgSO_4$. The solution was concentrated to 5 mL and poured into 30 mL of methanol and then filtered into a Soxhlet thimble. Soxhlet extraction was performed with methanol, hexanes, and chloroform. The polymer was recovered from the chloroform fraction by rotary evaporation. Finally, the polymer was further purified by size exclusion column chromatography over Bio-Rad Bio-Beads S = X1 eluting with chloroform to afford a solid. The solid was dried under vacuum overnight. The yield and molecular weight of the polymers are as follows. PBDTT-TEG, yield = 48%, M_n = 57.9 kDa, PDI = 2.36; ^{1}H NMR ($CDCl_3$, 400 MHz): δ (ppm) = 7.63 (br, 2H), 7.18 (br, 2H), 4.48 (br, 4H), 3.94 (br, 4H), 3.82–3.79 (br, 4H), 3.71 (br, 4H), 3.56 (br, 4H), 3.37 (br, 6H). Elemental analysis called (%) for $C_{28}H_{34}O_8S_3$: C56.54, H5.76; found: C56.10, H5.32. PBDTT-EH, yield = 45%, M_n = 42.4 kDa, PDI = 2.35; ^{1}H NMR ($CDCl_3$, 400 MHz): δ (ppm) = 7.52 (br, 2H), 6.99 (br, 2H), 4.19 (br, 4H), 2.26 (br, 2H), 2.02–1.56 (br, 16H), 0.92–0.86 (br, 32H). Elemental analysis called (%) for $C_{30}H_{38}O_2S_3$: C68.40, H7.27; found: C67.88, H7.48.

2.3 PFET device fabrication and measurement

PFETs were constructed on octadecyltrichlorosilane (OTS)-modified SiO_2/Si substrates with top-contact configuration. The 10 mg ml^{-1} ODCB solutions of the polymers were spin-coated on the substrates in air at room temperature. The source and drain electrodes were patterned through the mask using thermal evaporation method. The channel length were 100 μm and the ratio of channel width to channel length W/L = 110. The mobility in the saturation regime was determined using the equation: $I_{DS} = (\mu_{FET}WC_i/2L)(V_G - V_T)^2$,[42] where I_{DS} is the drain-source current in the saturated regime, μ_{FET} is the field-effect mobility, W the channel width, L the channel length, C_i the capacitance of SiO_2 dielectric layer, V_G the gate voltage and V_T the threshold voltage.

2.4 PSC device fabrication and measurement

PSC devices with the structure ITO/poly(3,4-ethylenedioxythiophene): poly(styrenesulfonate) (PEDOT:PSS)/polymers:$PC_{71}BM$(w/w)/Ca/Al were fabricated as follows: After spin-coating a 40 nm layer of PEDOT:PSS onto cleaned ITO-coated glass substrates, the polymer/$PC_{71}BM$ solution used in this study for spin-coating was 10 mg mL^{-1} ODCB/$CHCl_3$ (2 : 3) solutions. In order to compare the device parameters, all of the optimized devices had active-layer thicknesses of ~100 nm. The devices were completed by evaporating Ca/Al metal electrodes with an area of 4 mm^2 as defined by masks. To optimize device performance, different D/A weight ratios (1 : 1 to 1 : 5) were used in binary devices and specific D/A weight ratios ratio (1 : 3) were used in ternary devices during the device fabrication process.

3. Results and discussion

The optical and electrochemical properties of the polymers were further analyzed. As shown in Fig. 1, both polymers showed a similar absorption in the 300–600 nm area. The absorption spectrum of PBDTT-TEG in chloroform solution and film showed absorption maxima at 500/538 and 515/545 nm, respectively. While the PBDTT-EH in chloroform solution and film showed maximum absorption peaks at 499/535 and 505/543 nm, respectively. The peak positions of PBDTT-EH are slightly blue-shifted in the low energy range which could be explained as the bulkier side chains and more steric interactions inhibiting backbone planarity.[27] The spectra of the two polymers showed a similar red shift from solution to film, which was attributed to their similar

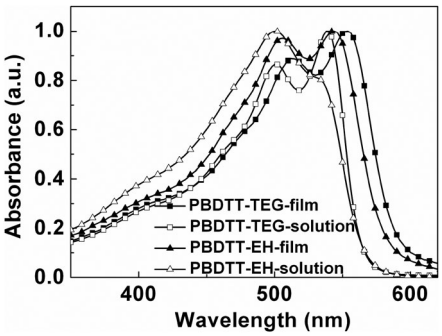

Fig. 1 Normalized absorption spectra of polymers as a film and in chloroform solution.

structure and stacking state. On the other hand, the absorption edge of PBDTT-TEG (595 nm) was larger than that of PBDTT-EH (587 nm) in films, indicating the efficient conjugation length of PBDTT-TEG was bigger than the PBDTT-EH. This was consistent with the assumption that TEG side chains did not cause a detrimental steric twist of the polymer out of planarity which would be beneficial for the π–π stacking.[33]

The electrochemical properties of the polymers were investigated by cyclic voltammetry (CV). As shown in Fig. 2, the polymers showed similar reversible p-doping/dedoping (oxidation/re-reduction) and n-doping/dedoping (reduction/reoxidation) processes. The energy levels of the highest occupied molecular orbital (HOMO) an dthe lowest unoccupied molecular orbital (LUMO) can be calculated from the onset oxidation and reduction potentials according to the equations: HOMO = $-e(E_{on}^{ox} + 4.71)$ and LUMO = $-e(E_{on}^{red} + 4.71)$ (eV).[43] The electrochemical band gaps (E_g^{ec}) can be calculated from the equation: $E_g^{ec} = (E_{on}^{ox} - E_{on}^{red})$ (eV). The results of the CV were also listed in Table 1. The HOMO levels and the LUMO levels of PBDTT-TEG and PBDTT-EH were estimated to be at −4.99, −5.15 eV and −2.66, −2.59 eV, respectively. It was found that the HOMO level of PBDTT-TEG was higher than that of PBDTT-EH, which should be attributed to the electron-rich property of the TEG groups. This higher HOMO level was considered detrimental for obtaining high V_{oc} in photovoltaic applications containing the polymers as donors, because the V_{oc} value was closely related to the difference between the HOMO level of the donor and the LUMO level of the acceptor in BHJ PSCs.[2,44] The band gap of PBDTT-TEG (2.33 eV) was narrower than that of PBDTT-EH (2.56 eV), which may be attributed to the better stacking properties and smaller steric hindrance of the TEG side chain compared with the branched one.

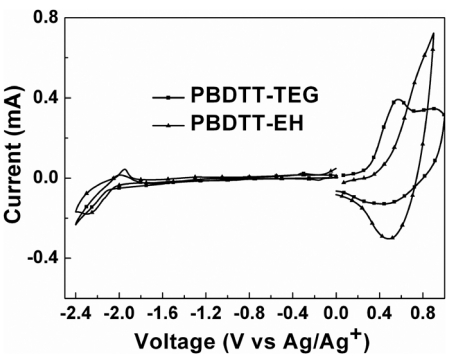

Fig. 2 Cyclic voltammograms of polymer films on a platinum electrode in 0.1 mol L^{-1} Bu_4NPF_6 (CH_3CN) solution.

Table 1 Optical and electrochemical properties of polymers

Polymers	UV-vis absorption spectra: Solution λ_{max} (nm)	Film λ_{max} (nm)	E_g^{ec} (eV)	HOMO (eV)	LUMO (eV)
PBDTT-TEG	500/538	515/545	2.33	−4.99	−2.66
PBDTT-EH	499/535	505/543	2.56	−5.15	−2.59

The PFETs with a conventional bottom-contact and bottom-gate configuration were fabricated using the two polymers as the active layer. Fig. 3 showed the representative transfer and output current–voltage plots for the PFETs fabricated on an OTS-treated Si/SiO_2 (300 nm) substrate. The devices showed a typical *p*-type transporting characteristic measured under ambient conditions. The PBDTT-EH-based PFETs exhibited relatively lower hole mobility of 5.1×10^{-4} cm^2 V^{-1} s^{-1} with an on/off ratio of 1.8×10^3, while the PBDTT-TEG-based devices showed a higher hole mobility of 4.1×10^{-3} cm^2 V^{-1} s^{-1} with a higher on/off ratio about 3.0×10^4. The nearly one order of magnitude higher mobility of the PBDTT-TEG could be induced by the better conjugation along the backbone and better π–π stacking. This relatively high mobility was absolutely necessary to reach high current density (J_{sc}) and FF of the PSC devices as previous reported in the literatures.[3]

PSCs were then fabricated with a conventional sandwich structure, where the active layer was composed of polymers as the donor and $PC_{71}BM$ as the acceptor with a general structure of indium/ITO/PEDOT:PSS/polymer:$PC_{71}BM$ (w/w)/Ca/Al under simulated AM 1.5 G illumination (100 mW cm^{-2}), where PEDOT:PSS was used to facilitate the hole extraction. Fig. 4a shows the typical current density–voltage (*J*–*V*) curves of the binary devices. Optimizations were carried out by altering the polymer:$PC_{71}BM$ ratios, film thickness and thermal annealing temperatures. The best devices for PBDTT-TEG and PBDTT-EH demonstrated V_{oc} of 0.47 and 0.72 V, J_{sc} of 6.82 and 4.18 mA cm^{-2}, and FF of 0.44 and 0.53, with film thickness ∼100 nm. The resulting PCEs thus reached 1.42% and 1.60%. The device performance of PBDTT-EH was very coincident with the efficiency of similar polymers reported in previous literature.[45] It was found that both the polymers exhibited the best performance when the D/A ratio was 1 : 3. However, the PCEs of the devices were limited to less than 1% when the amount of acceptor continuously increased. The corresponding best V_{oc}, J_{sc}, FF and PCE values of the devices in different conditions are summarized in Table 2. The two polymer–fullerene binary blends gave significantly different values of V_{oc} (∼0.50 V for PBDTT-TEG and ∼0.70 V for PBDTT-EH) due to the different positions of the HOMO levels (−4.99 eV for PBDTT-TEG and −5.15 eV for PBDTT-EH, respectively). The V_{oc} value was closely related to the difference between the LUMO level of the acceptor and the HOMO level of the donor in BHJ PSCs.[2,3,8]

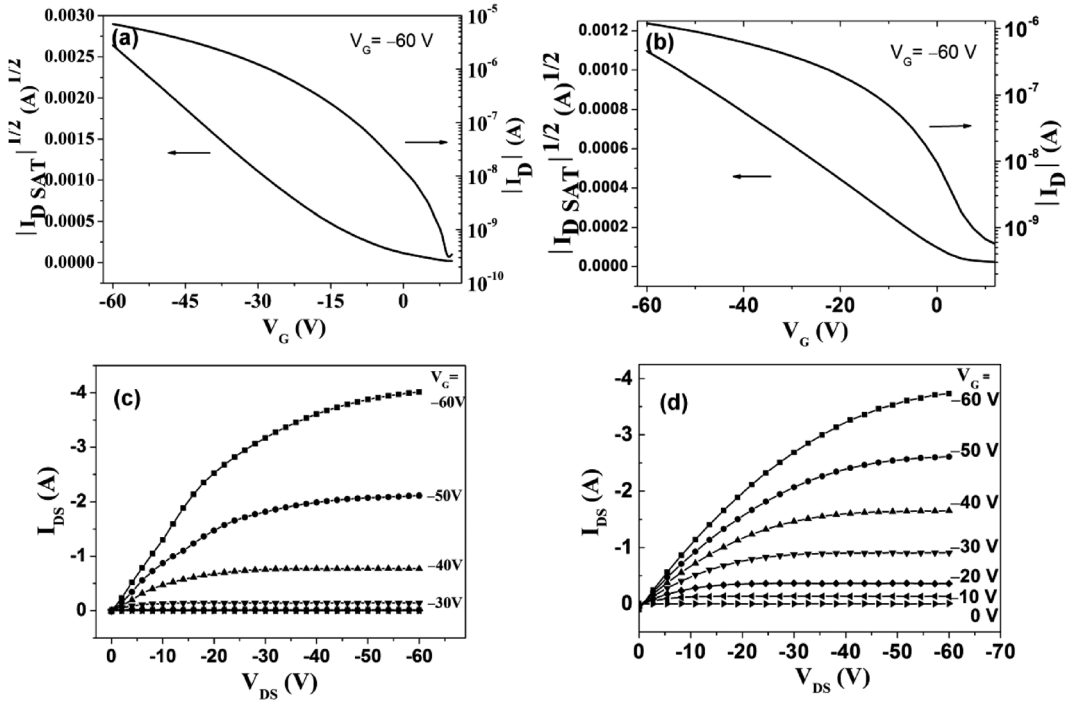

Fig. 3 The typical PFET performance based on the two polymers:, (a), (b) are the transfer curves for PBDTT-TEG and PBDTT-EH; (c), (d) are the output curves for PBDTT-TEG and PBDTT-EH.

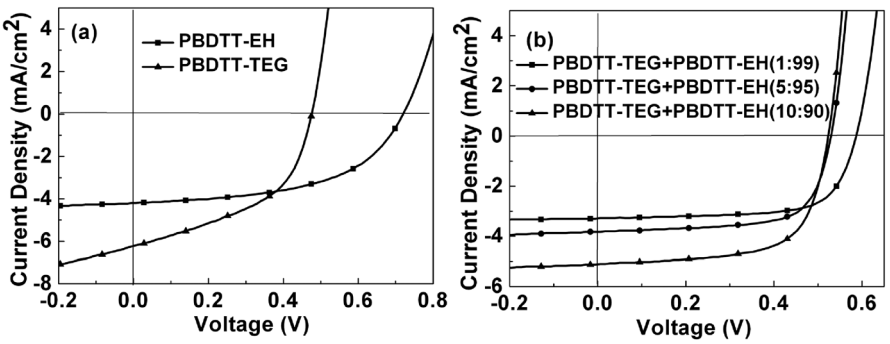

Fig. 4 Typical *J*–*V* curve for (a) binary devices and (b) different ratios of ternary blend devices under an illumination of AM 1.5G, 100 mW cm^{-2}.

Obviously, the J_{sc} values of PBDTT-TEG devices were higher than those of PBDTT-EH, which should arise from the red-shifted absorption spectrum and the higher carrier mobility.[3,46]

As the two polymers possessed similar energy levels, the same backbone structure and a suitable high mobility, their ternary blend devices were assumed to have higher PSC

Table 2 Photovoltaic parameters of PSCs based on polymer/$PC_{71}BM$ binary films

Polymer	Polymer : $PC_{71}BM$ ratio	Active layer thickness (nm)	Annealing temperature (°C)	V_{oc} (V)	J_{sc} (mA cm^{-2})	FF (%)	η (%)
PBDTT-TEG	1 : 1	90	100	0.51	5.04	41.6	1.07
	1 : 2	95	RT[a]	0.48	5.27	45.0	1.14
	1 : 3	95	RT	0.47	6.82	44.3	1.42
	1 : 4	98	RT	0.49	4.49	38.2	0.84
PBDTT-EH	1 : 1	100	RT	0.71	3.65	43.6	1.13
	1 : 2	96	80	0.73	3.19	60.0	1.40
	1 : 3	98	110	0.72	4.18	53.1	1.60
	1 : 4	92	RT	0.70	3.16	39.8	0.88

[a] Room temperature.

performance. We suspected that the PBDTT-TEG were more likely to become entangled with the PBDTT-EH polymer chains, thereby utilizing its better charge transport property and good crystallinity. PSC devices containing ternary blends in the conventional device configuration ITO/PEDOT:PSS/(PBDTT-TEG:PBDTT-EH, w/w):$PC_{71}BM$(1 : 3)/Ca/Al were fabricated by blend with different ratios of PBDTT-TEG into PBDTT-EH, and the results are showed in Table 3. Fig. 4b shows the typical *J–V* curves of the ternary devices. J_{sc} and FF values of the three-component solar cells showed an obviously increase comparing with the PBDTT-EH binary ones. When the ratio of PBDTT-TEG : PBDTT-EH was 10 : 90, the gain of FF and J_{sc} over-compensated the V_{oc} losses, which resulted in an increase in overall efficiency. The distinct increase of the FF value could be attributed to balanced, trap-free charge transport through the bulk and favorable morphology. It was highly possible that the PBDTT-TEG with high mobility and good crystallinity served as an additional charge transport channel in the ternary device, to facilitate charge transport and consequently enhance the efficiency. Other concentrations of PBDTT-TEG in PBDTT-EH from 20–99% were also investigated. Unfortunately, the PCE values decreased rapidly when a large amount (greater than 30%) of PBDTT-TEG was blended into the PBDTT-EH. And the V_{oc} values decreased to under 0.47 eV (not listed), like some other conventional multi-blend systems where the observed V_{oc} decreased to the smaller V_{oc} of the corresponding binary blends.[12]

The X-ray diffraction (XRD) patterns of the PBDTT-TEG, PBDTT-EH and the blend samples were recorded to validate their crystallinity and structures in the solid state (Fig. 5). The diffraction peaks of PBDTT-TEG and PBDTT-EH were at 2θ = 5.24° and 5.66°, corresponding to interchain *d*-spacings of 16.86 and 15.61 Å, respectively, which were referenced as (100) reflections. The peak of PBDTT-TEG : PBDTT-EH (10 : 90) blend exhibited a relatively broad diffraction peak from 5.24° to 5.66°. Otherwise, peaks corresponding to the interchain distance for polymers were observed with different intensities, indicating that PBDTT-TEG has much better crystallinity than PBDTT-EH. This was consistent with the point that the TEG side chains benefited the crystallinity. However, PBDTT-TEG : PBDTT-EH (10 : 90) blend showed a similar intensity as PBDTT-EH film, which demonstrated that a small amount of PBDTT-TEG blend into PBDTT-EH film would bring a slight change and maybe just fine tuning of the resultant crystallinity.

Table 3 Photovoltaic parameters of PSCs based on different ratio of (PBDTT-TEG:PBDTT-EH) as donor and $PC_{71}BM$ as acceptor (D/A was 1 : 3)

PBDTT-TEG : PBDTT-EH	Active layer thickness (nm)	Annealing temperature (°C)	V_{oc} (V)	J_{sc} (mA cm^{-2})	FF (%)	η (%)
1 : 99	92	RT[a]	0.59	3.30	70.3	1.37
3 : 97	96	100	0.53	3.81	68.8	1.39
5 : 95	96	RT	0.51	5.17	66.0	1.74
10 : 90	98	RT	0.52	5.14	66.2	1.77
15 : 85	95	RT	0.50	4.38	57.6	1.26
30 : 70	100	110	0.46	5.22	40.0	0.96

[a] Room temperature.

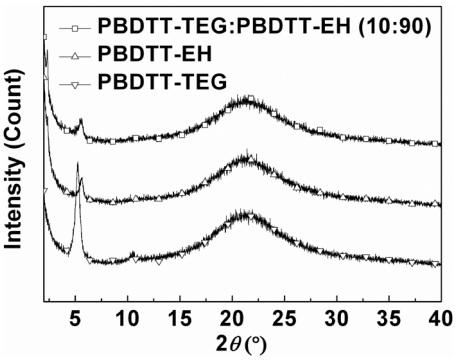

Fig. 5 XRD patterns of PBDTT-TEG : $PC_{71}BM$ (1 : 3), PBDTT-EH : $PC_{71}BM$ (1 : 3) and (PBDTT-TEG : PBDTT-EH, 10 : 90):$PC_{71}BM$ (1 : 3) spin coated on the quartz substrate.

On the other hand, film morphology control and formation of a nanoscale interpenetrating network *via* phase separation tuning was one of the critical issues to achieve high efficiency of BHJ PSCs.[47,48] To understand why blending good crystalline PBDTT-TEG into PBDTT-EH could influence the performance in the ternary devices, atomic force microscopy (AFM) was used to further characterize the surface morphology of the active layer. As shown in Fig. 6, an obvious difference in surface morphology could be found in the binary and ternary blend topography images. All the films showed smooth and bicontinuous morphology, which suggested that both of the polymers were compatible with $PC_{71}BM$ molecules. The PBDTT-TEG/$PC_{71}BM$ (1 : 3) blend film showed no significant aggregation (Fig. 6a). There were some pin-like domains in the PBDTT-TEG blend film. It should come from the volatilization of solvent in polymer material which has large viscosity. In contrast, clear aggregation domains with sizes of hundreds of nanometers could be observed from the image of PBDTT-EH/$PC_{71}BM$ blend and PBDTT-TEG : PBDTT-EH (10 : 90)/$PC_{71}BM$ film (Fig. 6b and c), indicating the PBDTT-EH was prone to aggregate when

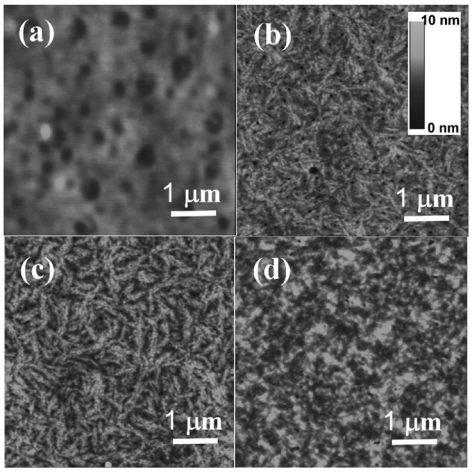

Fig. 6 Tapping mode AFM topography image (a) of PBDTT-TEG/$PC_{71}BM$ (1 : 3) blended film; (b) of PBDTT-EH/$PC_{71}BM$ (1 : 3) blend film; (c) of (PBDTT-TEG : PBDTT-EH, 10 : 90)/$PC_{71}BM$ (1 : 3) blend film; (d) of (PBDTT-TEG : PBDTT-EH, 30 : 70)/$PC_{71}BM$ (1 : 3) blend film. The dimension of the images is 5 × 5 μm^2.

blended with $PC_{71}BM$. Previous work reported that TEG group with good crystallization would induce other components crystallizing on the surface when blended together.[49] Compared to PBDTT-EH/$PC_{71}BM$ binary film, the PBDTT-TEG : PBDTT-EH (10 : 90)/$PC_{71}BM$ exhibited bigger and more clearly dense domains, probably due to the induced aggregated effect of PBDTT-TEG. This slightly better crystalline morphology was very necessary to obtain large-area electron D–A interfaces to dissociate the excitons into free charges for pursuing a high photocurrent.[4] The improvement of FF values and overall PCE of the ternary blend were proposed to be attributed to the optimized phase separation compared to the binary blends. However, when a bigger amount (>10%) of PBDTT-TEG blended into PBDTT-EH, the film showed amorphous morphology and no self-assembled structures could be found (see Fig. 6d), which probably led the rapid decline of corresponding PSC performance.

4. Conclusions

In summary, we have fabricated ternary blend BHJ PSCs containing two polymers with TEG- and ethylhexyl-substituted BDT units as donor and $PC_{71}BM$ as acceptor. In this ternary blend system, PBDTT-TEG acts as the ''guest'' to improve the morphology and charge transport property of the ''host'' PBDTT-EH-based BHJ. Devices were tested at different polymer ratios and showed uniformly high FF values greater than 0.6 with a small amount of guest polymer blending into the host polymer. It was believed that additional higher mobility polymer would supply extra charge carriers which were able to transport to the anode *via* the better crystalline donor phase. To understand this improvement, the crystallinity and morphology of the binary and ternary samples were characterized, which showed that the best ternary device exhibited better crystalline aggregation and more proper phase separation than the binary devices. Though a detailed working mechanism in ternary devices remains to be further investigated, we believe ternary BHJ devices open a new avenue to accelerate the efficiency improvement of PSCs. We foresee that this approach might be of further use in other material systems to achieve even higher efficiency.

Acknowledgements

We acknowledge the financial support of the National Natural Science Foundation of China (Nos. 91027031, 21004015), the Ministry of Science and Technology of China (Nos. 2009CB930400, 2010DFB63530) and the Chinese Academy of Science (CAS).

Notes and references

1 J. E. Anthony, *Chem. Rev.*, 2006, **106**, 5028–5048.
2 Y. Li, *Acc. Chem. Res.*, 2012, **45**, 723–733.
3 J. W. Chen and Y. Cao, *Acc. Chem. Res.*, 2009, **42**, 1709–1718.
4 P. M. Beaujuge and J. M. J. Frechet, *J. Am. Chem. Soc.*, 2011, **133**, 20009–20029.
5 B. C. Thompson and J. M. J. Frechet, *Angew. Chem., Int. Ed.*, 2008, **47**, 58–77.
6 A. C. Arias, J. D. MacKenzie, I. McCulloch, J. Rivnay and A. Salleo, *Chem. Rev.*, 2010, **110**, 3–24.
7 G. Dennler, M. C. Scharber and C. J. Brabec, *Adv. Mater.*, 2009, **21**, 1323–1338.
8 G. Li, R. Zhu and Y. Yang, *Nat. Photonics*, 2012, **6**, 153–161.
9 L. J. Huo, J. H. Hou, S. Q. Zhang, H. Y. Chen and Y. Yang, *Angew. Chem., Int. Ed.*, 2010, **49**, 1500–1503.
10 Y. Y. Liang, D. Q. Feng, Y. Wu, S. T. Tsai, G. Li, C. Ray and L. P. Yu, *J. Am. Chem. Soc.*, 2009, **131**, 7792–7799.
11 Y. Y. Liang, Y. Wu, D. Q. Feng, S. T. Tsai, H. J. Son, G. Li and L. P. Yu, *J. Am. Chem. Soc.*, 2009, **131**, 56–57.
12 P. P. Khlyabich, B. Burkhart and B. C. Thompson, *J. Am. Chem. Soc.*, 2011, **133**, 14534–14537.
13 T. A. M. Ferenczi, C. Muller, D. D. C. Bradley, P. Smith, J. Nelson and N. Stingelin, *Adv. Mater.*, 2011, **23**, 4093–4097.
14 Z. Z. Sun, K. Xiao, J. K. Keum, X. Yu, K. L. Hong, J. Browning, I. N. Ivanov, J. H. Chen, J. Alonzo, D. W. Li, B. G. Sumpter, E. A. Payzant, C. M. Rouleau and D. B. Geohegan, *Adv. Mater.*, 2011, **23**, 5529–5535.
15 S. Honda, H. Ohkita, H. Benten and S. Ito, *Chem. Commun.*, 2010, **46**, 6596–6598.
16 M. Koppe, H. J. Egelhaaf, G. Dennler, M. C. Scharber, C. J. Brabec, P. Schilinsky and C. N. Hoth, *Adv. Funct. Mater.*, 2010, **20**, 338–346.
17 B. C. Thompson, Y. G. Kim and J. R. Reynolds, *Macromolecules*, 2005, **38**, 5359–5362.
18 C. H. Chen, C. H. Hsieh, M. Dubosc, Y. J. Cheng and C. S. Su, *Macromolecules*, 2010, **43**, 697–708.
19 R. C. Mulherin, S. Jung, S. Huettner, K. Johnson, P. Kohn, M. Sommer, S. Allard, U. Scherf and N. C. Greenham, *Nano Lett.*, 2011, **11**, 4846–4851.
20 G. Adam, A. Pivrikas, A. M. Ramil, S. Tadesse, T. Yohannes, N. S. Sariciftci and D. A. M. Egbe, *J. Mater. Chem.*, 2011, **21**, 2594–2600.
21 P. P. Khlyabich, B. Burkhart and B. C. Thompson, *J. Am. Chem. Soc.*, 2012, **134**, 9074–9077.
22 L. Q. Yang, H. X. Zhou, S. C. Price and W. You, *J. Am. Chem. Soc.*, 2012, **134**, 5432–5435.
23 L. J. Huo, S. Q. Zhang, X. Guo, F. Xu, Y. F. Li and J. H. Hou, *Angew. Chem., Int. Ed.*, 2011, **50**, 9697–9702.
24 H. Pan, Y. Wu, Y. Li, P. Liu, B. S. Ong, S. Zhu and G. Xu, *Adv. Funct. Mater.*, 2007, **17**, 3574–3579.
25 Y. Zhang, S. K. Hau, H. L. Yip, Y. Sun, O. Acton and A. K. Y. Jen, *Chem. Mater.*, 2010, **22**, 2696–2698.
26 L. J. Huo and J. H. Hou, *Polym. Chem.*, 2011, **2**, 2453–2461.
27 C. Piliego, T. W. Holcombe, J. D. Douglas, C. H. Woo, P. M. Beaujuge and J. M. J. Frechet, *J. Am. Chem. Soc.*, 2010, **132**, 7595–7597.
28 Z. Li, S. W. Tsang, X. M. Du, L. Scoles, G. Robertson, Y. G. Zhang, F. Toll, Y. Tao, J. P. Lu and J. F. Ding, *Adv. Funct. Mater.*, 2011, **21**, 3331–3336.

29 B. Burkhart, P. P. Khlyabich and B. C. Thompson, *Macromolecules*, 2012, **45**, 3740–3748.
30 K. Lu, J. Fang, Z. Yu, H. Yan, X. Zhu, Y. Zhang, C. He and Z. Wei, *Org. Electron.*, 2012, **13**, 3234–3243.
31 R. D. McCullough, *Adv. Mater.*, 1998, **10**, 93–116.
32 C. S. Velazquez, J. E. Hutchison and R. W. Murray, *J. Am. Chem. Soc.*, 1993, **115**, 7896–7897.
33 J. Roncali, P. Marque, R. Garreau, F. Garnier and M. Lemaire, *Macromolecules*, 1990, **23**, 1347–1352.
34 S. C. Chien, F. C. Chen, M. K. Chung and C. S. Hsu, *J. Phys. Chem. C*, 2012, **116**, 1354–1360.
35 J. W. Jung, J. W. Jo and W. H. Jo, *Adv. Mater.*, 2011, **23**, 1782–1787.
36 F. C. Chen and S. C. Chien, *J. Mater. Chem.*, 2009, **19**, 6865–6869.
37 Q. D. Tai, J. H. Li, Z. K. Liu, Z. H. Sun, X. Z. Zhao and F. Yan, *J. Mater. Chem.*, 2011, **21**, 6848–6853.
38 C. Z. Li, C. C. Chueh, H. L. Yip, K. M. O. Malley, W. C. Chend and A. K.-Y. Jen, *J. Mater. Chem.*, 2012, **22**, 8574–8578.
39 J. Y. Jeng, M. W. Lin, Y. J. Hsu, T. C. Wen and T. F. Guo, *Adv. Energy Mater.*, 2011, **1**, 1192–1198.
40 F. Zhang, M. Ceder and O. Inganas, *Adv. Mater.*, 2007, **19**, 1835–1838.
41 D. W. Slocum and P. L. Gierer, *J. Org. Chem.*, 1976, **41**, 3668–3673.
42 K. Lu, C. A. Di, H. X. Xi, Y. Q. Liu, G. Yu, W. F. Qiu, H. J. Zhang, X. Gao, Y. Liu, T. Qi, C. Y. Du and D. B. Zhu, *J. Mater. Chem.*, 2008, **18**, 3426–3432.
43 Q. J. Sun, H. Q. Wang, C. H. Yang and Y. F. Li, *J. Mater. Chem.*, 2003, **13**, 800–806.
44 S. Gunes, H. Neugebauer and N. S. Sariciftci, *Chem. Rev.*, 2007, **107**, 1324–1338.
45 J. H. Hou, M. H. Park, S. Q. Zhang, Y. Yao, L. M. Chen, J. H. Li and Y. Yang, *Macromolecules*, 2008, **41**, 6012–6018.
46 V. Coropceanu, J. Cornil, D. A. da Silva, Y. Olivier, R. Silbey and J. L. Bredas, *Chem. Rev.*, 2007, **107**, 926–952.
47 X. D. Dang, A. B. Tamayo, J. Seo, C. V. Hoven, B. Walker and T. Q. Nguyen, *Adv. Funct. Mater.*, 2010, **20**, 3314–3321.
48 Y. Zhang, J. Y. Zou, H. L. Yip, Y. Sun, J. A. Davies, K. S. Chen, O. Acton and A. K. Y. Jen, *J. Mater. Chem.*, 2011, **21**, 3895–3902.
49 K. Zhao, Z. C. Ding, L. J. Xue and Y. C. Han, *Macromol. Rapid Commun.*, 2010, **31**, 532–538.